CHAPTER 4

MAGNETIZATION DYNAMICS

William E. Bailey
Materials Science and Engineering, Department of Applied Physics and Applied Mathematics, Columbia University, New York, USA

4.1 LANDAU–LIFSHITZ–GILBERT EQUATION

The Landau–Lifshitz–Gilbert (LLG) equation for magnetization dynamics includes two types of motion: *precession* and *relaxation* (or *damping*). Historical context for the equation is given in Section 4.1.3. Section 4.1.3.1 shows how the LLG equation can be motivated intuitively through magnetomechanical experiments and how additional terms (such as those resulting from spin-torque) can be added to the equation of motion. In Section 4.1.3.2, we show how the Landau–Lifshitz (LL) and Landau–Lifshitz–Gilbert damping terms are equivalent in terms of the resulting motion and can be used interchangeably.

4.1.1 Introduction

Our direct experience with magnets tells us about the final state of magnetization dynamics. The magnetization $\mathbf{M}$ of a soft ferromagnetic material tends to align with applied magnetic fields $\mathbf{H}$, minimizing the Zeeman energy density,

$$U = -\mu_0 \mathbf{M} \cdot \mathbf{H}, \tag{4.1}$$

where μ_0 is the permeability of free space.

One might then guess that the *full motion* of $\mathbf{M}$, or $\dot{\mathbf{M}}$ (where the dot denotes a derivative with respect to time), describes rotation along a direct, energy-minimizing path. However, the dynamics of magnetization $\dot{\mathbf{M}}$ have two terms rather than only one, and the energy-minimizing term, *relaxation*, is usually one or two orders of magnitude smaller than an energy-preserving term, the *precession*. For precessional motion only, no energy is lost; $U = -\mu_0 \mathbf{M} \cdot \mathbf{H}$ remains constant as the magnetization $\mathbf{M}$ simply rotates around the field $\mathbf{H}$. The precession and relaxation terms were written first by Landau and Lifshitz in 1935 (1).

Introduction to Magnetic Random-Access Memory, First Edition. Edited by Bernard Dieny, Ronald B. Goldfarb, and Kyung-Jin Lee.

4.1.2 Variables in the Equation

Before describing the LL equation, we define the variables involved, the choice of which contains important assumptions about the physics of magnetization motion.

Reduced Magnetization Ferromagnets are distinguished by their spontaneous magnetic order. For any magnetic material, the magnetization can be written as $M = N_v\langle\mu\rangle$, where N_v is the volume density of dipole moments (in units of m^{-3}) and $\langle\mu\rangle$ is an ensemble average dipole moment ($\mathrm{A\,m}^2$), taken along the direction of the applied field. The magnitude $|\mu|$ is constant in a ferromagnet, independent of applied field $\mathbf{H}$ for constant temperature. Within a single *domain*, the magnetization is equal to the saturation magnetization $M = M_s = N_v|\mu|$. The direction of $\mathbf{M}$ can vary; the influence of $\mathbf{H}$ is to change the direction. It becomes sensible to define the *reduced magnetization* $\mathbf{m}$,

$$\mathbf{m} \equiv \mathbf{M}/M_s, \tag{4.2}$$

as a unit vector in the magnetization direction. Magnetization dynamics are thus *rotational*, at right angles to $\mathbf{m}$, describing trajectories on the unit sphere,

$$\mathbf{m} \cdot \dot{\mathbf{m}} = 0. \tag{4.3}$$

Clearly, in ferromagnetic materials the demagnetized state $\mathbf{M} = 0$ is possible, but only as a large-scale average over domains, averaging to zero magnetization. Micromagnetic calculations make the similar assumption that in each finite element, $\mathbf{m}$ is a unit vector, M_s does not change, and the task is to calculate $\mathbf{m}(\mathbf{r})$ for all spatial coordinates $\mathbf{r}$.

Effective Field The magnetization direction $\mathbf{m}$ influences the energy of a ferromagnet in several ways. The Zeeman energy, Eq. (4.1), created by an applied external field $\mathbf{H_b}$, is one energy term, but the variation of $\mathbf{m(r)}$ can create other terms as well. Anisotropies due to shape (dipolar fields), interaction with crystal fields (magnetocrystalline anisotropy, induced anisotropy in alloys), stress, and exchange, all have different possible energy terms. The most convenient way to treat these additional energies is through the definition of an *effective field* acting on particle i:

$$\mathbf{H}_{\mathbf{eff}}^{\mathbf{i}} = -\frac{1}{\mu_0 M_s}\frac{\partial U_i}{\partial \mathbf{m}}. \tag{4.4}$$

Since magnetic fields directed along $\mathbf{m}$ cannot exert a torque to rotate the magnetization, they are not effective. A Cartesian basis for $\mathbf{H_{eff}}$ in three variables is thus less compact than a spherical basis:

$$\mathbf{H}_{\mathbf{eff}}^{\mathbf{i}} = -\frac{1}{\mu_0 M_s}\left(\frac{\partial U_i}{\partial m_x}\hat{\mathbf{x}} + \frac{\partial U_i}{\partial m_y}\hat{\mathbf{y}} + \frac{\partial U_i}{\partial m_z}\hat{\mathbf{z}}\right) \tag{4.5}$$

can be written more compactly as

$$\mathbf{H}_{\mathbf{eff}}^{\mathbf{i}} = -\frac{1}{\mu_0 M_s}\left(\frac{\partial U_i}{\partial \varphi}\hat{\boldsymbol{\varphi}} + \frac{1}{\sin\theta}\frac{\partial U_i}{\partial \theta}\hat{\boldsymbol{\theta}}\right), \tag{4.6}$$

where the derivative in r is not allowed. In the usual convention, the magnetization direction is $\hat{\mathbf{r}} = \cos\varphi \sin\theta\, \hat{\mathbf{x}} + \sin\varphi \sin\theta\, \hat{\mathbf{y}} + \cos\theta\, \hat{\mathbf{z}}$.

4.1.3 The Equation

In Landau and Lifshitz's original paper (1), they proposed the equation

$$\dot{\mathbf{s}}/\mu_0 = [\mathbf{fs}] + \lambda\{\mathbf{f} - (\mathbf{fs})\mathbf{s}/s^2\} \quad \text{(cgs)}. \tag{4.7a}$$

In modern notation, with $\mathbf{s} \to \mathbf{M}$ (spin magnetization), $\mu_0 \to |\gamma|$ (explicitly for $g_{eff} = 2$), $\mathbf{f} \to \mathbf{H_{eff}}$ (effective field; see Section 4.1.2), square brackets to cross products, and parentheses to dot products, we get

$$\frac{\dot{\mathbf{M}}}{|\gamma|} = \mathbf{H_{eff}} \times \mathbf{M} + \lambda\left[\mathbf{H_{eff}} - \left(\frac{\mathbf{H_{eff}} \cdot \mathbf{M}}{M_s^2}\right)\mathbf{M}\right] \quad \text{(cgs)}. \tag{4.7b}$$

In the 80 years since their paper was published, the equation stands uncorrected. Alternative forms proposed for the second (relaxation) term (see Section 4.1.3.2) turn out to be equivalent. The gyromagnetic ratio can be expressed in SI units as

$$\gamma = \frac{e}{2m_e} g_{eff}, \tag{4.8}$$

where e is the electronic charge and m_e is the electronic rest mass. Numerically, in SI, γ is

$$\gamma = \gamma_0\left(\frac{g_{eff}}{2}\right), \quad \gamma_0 = -2\pi \times 27.99\ \text{GHz/T}, \tag{4.9}$$

with $g_{eff} = 2$, because LL considered pure spin-moments only. The cgs form is numerically identical, but more conveniently expressed as $\gamma_0 = -2\pi \times 2.799$ MHz/Oe. The assumption $g_{eff} = 2$ has been relaxed in subsequent years and values of g_{eff} up to 2.2 have been established experimentally given the mostly quenched, but nevertheless finite amounts of orbital moment in magnetic materials (2). See Section 4.2.3 for details.

Modern treatments of the LL equation typically use an alternative form, although the original form is no less valid and is still used occasionally. Dividing Eq. (4.7b) by M_s, making use of the vector identity $\mathbf{a} \times \mathbf{b} \times \mathbf{c} = \mathbf{b}(\mathbf{a}\cdot\mathbf{c}) - \mathbf{c}(\mathbf{a} \cdot \mathbf{b})$, thus $-\mathbf{m} \times \mathbf{m} \times \mathbf{H_{eff}} = \mathbf{H} - \mathbf{m}(\mathbf{m} \cdot \mathbf{H_{eff}})$, and introducing the *dimensionless damping parameter* α, we can write

$$\dot{\mathbf{m}} = -|\gamma|\mathbf{m} \times \mathbf{H_{eff}} - \alpha|\gamma|(\mathbf{m} \times \mathbf{m} \times \mathbf{H_{eff}}) \quad \text{(cgs)}, \tag{4.10}$$

$$\dot{\mathbf{m}} = -\mu_0|\gamma|\mathbf{m} \times \mathbf{H_{eff}} - \alpha\mu_0|\gamma|(\mathbf{m} \times \mathbf{m} \times \mathbf{H_{eff}}) \quad \text{(SI)}. \tag{4.11}$$

The dimensionless damping α (the same in both unit systems) can also be expressed as a rate λ:

$$\lambda \equiv |\gamma| M_s \alpha \quad \text{(cgs)}, \tag{4.12}$$

$$\lambda \equiv \frac{1}{4\pi}|\gamma|\mu_0 M_s \alpha \quad \text{(SI)}, \tag{4.13}$$

also defined here to have the same value in s^{-1} for both cgs and SI units. Alternative definitions of λ in SI units can differ by a factor of 4π; see Appendix of Ref. 3.

4.1.3.1 Precessional Term The first term of the LL equation is conservative. All energy stored in the magnetization system and its interactions with the lattice, expressed through the energy in the effective field, $U = -\mu_0 M_s \mathbf{m} \cdot \mathbf{H}_{eff}$, remains stored under operation of this term. Because the precessional term is dominant, constant-energy lines for $\mathbf{m}(\theta,\varphi)$ can be a good approximation for trajectories.

The form for the precessional term can be derived from Ehrenfest's theorem in quantum mechanics, as shown in elementary texts such as Ref. 4. We will instead motivate the precessional term semiclassically, through the Einstein-de Haas experiments (5).

Einstein-de Haas Experiments Einstein showed experimentally that there is a real connection between magnetization $\mathbf{M}$ and angular momentum $\mathbf{L}$. The magnetization of a cylinder of soft iron was suspended by a thin wire. An external solenoid coil reversed the magnetization, changing it by $\Delta M = 2M_s$ along its axis. The reversal caused the cylinder to rotate around its axis. The ratio between the mechanical angular momentum and magnetic angular momentum was identified as γ, where $\Delta\mathbf{M} = \gamma\Delta\mathbf{L}$. This relation can be generalized to a dynamical equation. The time derivative of both sides yields

$$\dot{\mathbf{M}} = \gamma\boldsymbol{\tau}, \quad \dot{\mathbf{M}} = \gamma\mu_0 \mathbf{M} \times \mathbf{H}, \tag{4.14}$$

where $\boldsymbol{\tau}$ is a mechanical torque on the body. Here, we substitute the torque on a point dipole per unit volume (magnetization) in a uniform field, $\boldsymbol{\tau} = \mu_0 \mathbf{M} \times \mathbf{H}$, appropriate under the single-domain approximation detailed earlier. Equation (4.14) provides an alternative and surprising derivation of the first term in the LL equation not mentioned in Ref. 1.

Magnetomechanical values of γ were in reasonable agreement with the free electron result e/m (e/mc in cgs). It is remarkable that Einstein was able to carry out these experiments in his spare time while he developed the theory of relativity, although students with similar ambitions should be aware that his measurements were found to be in error by a factor of 2 (6). Magnetomechanical and microwave resonance measurements of γ were later found by Barnett to agree within 10% (7); his measurements continued into the early 1950s (8).

Additional Torque Terms Novel terms to magnetization dynamics, such as the influence of spin-torque, can be added into the LLG. Both the torque and the magnetic moment are total, volume-summed quantities, so to convert an additional torque term to dynamics of reduced magnetization $\mathbf{m}$, the torque term needs to be expressed as

$$\dot{\mathbf{m}} = \cdots - \frac{|\gamma|}{StM_s}\boldsymbol{\tau} \quad \text{(cgs)}, \quad \dot{\mathbf{m}} = \cdots - \frac{|\gamma|}{St\mu_0 M_s}\boldsymbol{\tau} \quad \text{(SI)}. \tag{4.15}$$

Here, the volume of a thin film is taken as $S{\cdot}t$, where S is the area and t is the thickness.

4.1.3.2 Relaxation Term The relaxation term has been more controversial and more widely discussed in the years since LL's paper. LL added the term completely ad hoc in order to have the magnetization decay toward $\mathbf{H_{eff}}$. In the equivalent expression, Eq. (4.10), it is clear how relaxation operates geometrically: $\mathbf{m}\times\mathbf{H}$ gives the axis about which $\mathbf{m}$ needs to rotate to bring the $\mathbf{m}$ and $\mathbf{H}$ into alignment, and $\mathbf{m}$ moves at right angles to it.

Gilbert Form An alternative form for the damping term was proposed by Gilbert and Kelly in 1955 (9,10), allowing the new LL equation to be written as

$$\dot{\mathbf{m}} = -\mu_0|\gamma|\mathbf{m}\times\mathbf{H_{eff}} + \alpha(\mathbf{m}\times\dot{\mathbf{m}}). \tag{4.16}$$

This form is known as the *Landau–Lifshitz–Gilbert* equation. Gilbert justified the new damping term by claiming that the "higher" damping observed for $Ni_{81}Fe_{19}$ platelets would be better represented by a "viscous" term proportional to $\dot{\mathbf{m}}$. For low damping, $\alpha \ll 1$ (true for almost all known cases), it can be shown easily that the LL and LLG forms are equivalent. If the relaxation term to the motion is small compared with the precessional term, one can obtain Eq. (4.16) from Eq. (4.10) by substituting $\dot{\mathbf{m}} \approx |\gamma|\mathbf{m}\times\mathbf{H_{eff}}$.

Functional Equivalence of the LL and Gilbert Damping The identity between the LL and LLG forms is more exact than a small-damping approximation. Magnetization trajectories are equivalent for all angles subject to a small redefinition of γ. Decomposition of Eqs. (4.11 and 4.16) into spherical coordinates yields the directly integrable expressions:

$$\begin{bmatrix}\dot{\theta}\\ \dot{\varphi}\end{bmatrix} = \mu_0|\gamma|\begin{bmatrix}\alpha & 1\\ \dfrac{-1}{\sin\theta} & \dfrac{\alpha}{\sin\theta}\end{bmatrix}\begin{bmatrix}H_\theta^{eff}\\ H_\varphi^{eff}\end{bmatrix} \quad \text{(SI, LL)}, \tag{4.17}$$

$$\begin{bmatrix}\dot{\theta}\\ \dot{\varphi}\end{bmatrix} = \frac{\mu_0|\gamma|}{1+\alpha^2}\begin{bmatrix}\alpha & 1\\ \dfrac{-1}{\sin\theta} & \dfrac{\alpha}{\sin\theta}\end{bmatrix}\begin{bmatrix}H_\theta^{eff}\\ H_\varphi^{eff}\end{bmatrix} \quad \text{(SI, LLG)}, \tag{4.18}$$

so that LL and LLG trajectories are equivalent if we take $\gamma_{LL} = \gamma_{LLG}/\left(1+\alpha^2\right)$. Gilbert recognized the equivalence in an expanded version of his paper (10).

No physical behavior can be explained by the LLG that could not be explained by the LL, as long γ and α are both free parameters. The gyromagnetic ratio would need to be resolved to better than one part in α^{-2} to separate the expressions even in principle. Table 4.1 shows a best precision in measurement of γ to about 0.007, on the order of α for $Ni_{81}Fe_{19}$. While there may be formal reasons to prefer one form over another, a debate that continues (11), the difference between these forms would be quite challenging to resolve in an experiment. The LL form is more convenient for algebraic manipulations since the right side of the equation contains no terms in $\dot{\mathbf{m}}$.

Finally we note that λ, the relaxation rate (in units of s^{-1}) in the LL damping scheme, has an analogous rate G in the Gilbert damping scheme, with $\lambda = G$. These values can be used interchangeably. See Table 4.1 for values.

TABLE 4.1 Room-Temperature Values of Materials Parameters for Several Typical Ferromagnets and Ferromagnetic Alloys.

Material	g_{eff} (12,13)	$\mu_0 M_s$ (T) (14)	α_0 ($\times 10^{-3}$)	λ or G (MHz)
Fe	2.094 ± 0.02	2.1545	1.8	57 (15–17)
Co	2.170 ± 0.02	1.8173	8.5	170–280 (16)
Ni	2.185 ± 0.02	0.6165	23.3	220 (18)
$Ni_{81}Fe_{19}$ (Py)	2.129 ± 0.02	0.95 (19) – 1.07 (20)	7.0 (21)	98–111
$Co_{60}Fe_{20}B_{20}$ (20)	2.07	1.14	6.5 (20)	107
$Co_{72}Fe_{18}B_{10}$ (22)	2.07	1.76	6.0 (20)	153

Precision is no better than 1% for g_{eff} and no better than 5% for α and G.

4.2 SMALL-ANGLE MAGNETIZATION DYNAMICS

In this section, we consider small-angle rotations of the magnetization for in-plane magnetization. First, in Section 4.2.1, we see how the LLG can be linearized for small angles θ with respect to an in-plane equilibrium magnetization. Solutions for this equation under periodic driving are shown in Section 4.2.2. The corresponding experimental technique is ferromagnetic resonance (FMR), which measures the absorption of microwaves through the frequency-dependent susceptibility. FMR is the source of most data on the dynamical response of ferromagnetic materials and heterostructures. Experimental parameters, both in the "bulk" and possible modification through film surfaces (finite-size effects), are reviewed in Section 4.2.3. Solutions for pulsed magnetization motion, relevant for the beginning or end of switching processes, are shown in Section 4.2.4.

4.2.1 LLG for Thin-Film, Magnetized in Plane, Small Angles

We will treat the magnetization dynamics of an ultrathin film, relevant for magnetic random access memory (MRAM). Even for elements patterned to a 100 nm pillar, a 5 nm thick ferromagnetic film can be approximated reasonably well as a semi-infinite film. The magnetization is assumed to have its zero-field orientation in the y–z plane. We take the film normal to be $\hat{\mathbf{x}}$. The magnetization is assumed to be saturated along $\hat{\mathbf{z}}$ in the presence of external applied fields along $\hat{\mathbf{z}}$, an approximation strictly true in limiting cases (Note that full alignment is strictly true only in the case of pure hard axis or pure-easy axis alignment) (see Section 4.3).

Much of the interesting behavior in magnetization dynamics concerns only small excursions of the magnetization from its equilibrium direction. We introduce the following reduced variables (23):

$$\omega_M \equiv \mu_0 |\gamma| M_s, \quad \omega_H \equiv \mu_0 |\gamma| H'_z, \tag{4.19}$$

where $H'_z = H_b + H_K + \cdots$ is defined as an *effective field* including any uniaxial (or unidirectional) anisotropy fields maintaining the magnetization along the biased direction. (Surface anisotropy terms will be discussed later.) We can express

Eq. (4.11) in the form

$$\begin{bmatrix} \dot{m}_x \\ \dot{m}_y \end{bmatrix} = \begin{bmatrix} -\alpha(\omega_M + \omega_H) & -\omega_H \\ \omega_M + \omega_H & -\alpha\omega_H \end{bmatrix} \begin{bmatrix} m_x \\ m_y \end{bmatrix} + \begin{bmatrix} \alpha & 1 \\ -1 & \alpha \end{bmatrix} \begin{bmatrix} \gamma H_x^{eff} \\ \gamma H_y^{eff} \end{bmatrix}$$

under the assumption $m_x, m_y \ll 1$ and $m_z \simeq 1$.

This is the most compact form of the LL equation, valid for small angles. This system of two coupled ordinary differential equations in m_x, m_y can be converted to a single second-order ordinary differential equation in m_y by differentiating the first and substituting the second into the first. After some algebra, we can convert these equations into the classical equation for a driven harmonic oscillator,

$$\ddot{m}_y + \eta\dot{m}_y + \omega_0^2 m_y = f_0^2 \cos\omega t, \tag{4.20}$$

$$\eta = \alpha(\omega_M + 2\omega_H), \quad \omega_0 = \sqrt{\omega_H(\omega_H + \omega_M)}, \quad f_0^2 \approx (\omega_M + \omega_H)\gamma H_{y,0}, \tag{4.21}$$

where the α term in the drive is neglected. A similar equation could be written for m_x. Note that the relaxation rate η, resonant frequency ω_0, and driving amplitude f_0 are all functions of the applied field through ω_H.

Re-expanding the variables in SI units, we can write the *Kittel equation* for the resonant frequency of precession as

$$\upsilon_0 = \frac{\omega_0}{2\pi} = \frac{|\gamma_0|}{2\pi}\left(\frac{g_{eff}}{2}\right)\mu_0\sqrt{H_z'(H_z' + M_s)}. \tag{4.22}$$

4.2.2 Ferromagnetic Resonance

In their 1935 paper, Landau and Lifshitz worked through Eq. (4.7a), derived a correct expression for the susceptibility $\chi(\omega)$ for a sphere, and predicted a large enhancement of microwave power absorption on resonance—all far before any experimental observation of magnetic resonance. Rabi and coworkers at Columbia reported the first experimental observation of nuclear magnetic resonance (NMR) using time-of-flight techniques in 1938 (24). The observation of resonant absorption at microwave frequencies, relying on advances in radar technology (25), did not appear until 1945; the first observation of electron spin resonance (ESR) (26) was followed rapidly by the first observation of NMR in 1946 (27), and then by FMR later that year (28). The role of dipolar fields in increasing the in-plane resonance frequency for FMR (as $\gamma\sqrt{BH}$) was first understood by Kittel (29).

Microwave Susceptibility The absorption of microwaves in an insulating ferromagnet is found through the complex susceptibility $\chi''(\omega)$; eddy currents bring complications in conductive ferromagnets. From the equation for susceptibility in a forced harmonic oscillator, we can find $\chi(\omega)$ for the ferromagnetic thin film; neglecting terms in α (2),

$$\chi_{M,//} = \frac{M_y}{H_y} = \frac{M_s}{H_y}\frac{f_0^2}{\left(\omega_0^2 - \omega^2\right) + i\eta\omega} = \frac{\omega_M(\omega_M + \omega_H)}{\left(\omega_0^2 - \omega^2\right) + i\eta\omega}, \tag{4.23}$$

which can be expressed in terms of reduced variables,

$$h \equiv \frac{\omega_H}{\omega_M}, \quad h \equiv \frac{H_z'}{M_s}, \quad \Omega \equiv \frac{\omega}{\omega_M}, \quad \chi_M = \frac{h+1}{h(h+1) - \Omega^2 + i(1+2h)\alpha\Omega}. \tag{4.24}$$

On and near resonance, we can express $h = h_r + \Delta h$, where h_r is the field for resonance at fixed frequency Ω. We then have for the imaginary part of the susceptibility χ_M'', neglecting terms $\ddot{A}h^2 \ll 1$ and $\ddot{A}h \ll h_r$,

$$\chi_M'' \approx \alpha\Omega \frac{h_r + 1}{(1+2h_r)} \frac{1}{(\Delta h)^2 + \alpha^2\Omega^2}.$$

We see that there is a Lorenzian (peaked) enhancement of imaginary susceptibility (power absorption) at the resonant frequency $\omega = \omega_0$, by a maximum of α^{-1}. Expressing the full-width in field for which χ'' reaches half its peak value, we have

$$\Delta H(\omega) = \Delta H_0 + \frac{2\alpha}{|\gamma|}\omega \quad (cgs), \quad \mu_0 \Delta H(\omega) = \mu_0 \Delta H_0 + \frac{2\alpha}{|\gamma|}\omega \quad (\text{SI}) \tag{4.25}$$

to which we have added an inhomogeneous broadening term ΔH_0 that might arise due to large-scale magnetic disorder.

Extraction of Materials Parameters Equation (4.25) describes how to measure the damping α in a swept-field, variable frequency FMR experiment. The damping α is found through a linear fit to frequency-dependent linewidth $\Delta H(\omega)$, where α is given by the slope and ΔH_0 is given by the zero-frequency offset. (An alternative view holds that disorder combined with exchange coupling between grains can also produce a frequency-dependent linewidth (30), but these complications are generally exhausted at relatively low frequencies (10–20 GHz).) The range up to 70 GHz is best for materials such as Fe. Measurements in the range of 0–24 GHz are most reliable where ferromagnetic materials are very soft (easily magnetized) and there is little contribution from magnetocrystalline anisotropy (e.g., Permalloy (Py), $Ni_{81}Fe_{19}$).

The resonance position provides a good estimate of other materials parameters influencing the effective field. From Eq. (4.20) we have $\omega_0 = \mu_0\gamma\sqrt{H_z'\left(H_z' + M_s\right)}$. In the absence of surface anisotropy, the slope of $\omega(H_b)$ is determined primarily by the film magnetization M_s. In the presence of surface anisotropy (see Section 4.2.3.2), the slope of $\omega(H_b)$ contains a contribution from surface anisotropy. In either case, the offset of $\omega(H_b)$ provides a measure of H_K. For in-plane measurements, γ can be taken from the literature (12,13); see Table 4.1.

Eddy Currents Equation (4.25) cannot be used for the damping of thick metallic ferromagnetic films. Ament and Rado (31) have developed an expression for the equivalent permeability $\mu_{eff}(\omega)$ of semi-infinite films. The finite conductivity of the metal film implies a finite skin depth for microwaves; the skin depth is reduced compared with the nonmagnetic case by a factor $\mu_r^{-1/2} = \sqrt{1+\chi_M}$. The inhomogeneous magnetization profile in the ferromagnet gives rise to inhomogeneous

exchange fields, broadening the resonance. Experimental extraction of λ often failed in bulk whiskers (18) and oft-cited (32,33) low-temperature values of λ for Co and Fe are in fact poorly known. Accurate measurements of α in ferromagnetic metals were enabled only through the production of ultrathin ferromagnetic films, where the Rado-Ament analysis was not necessary. For films thinner than those hat support a spin wave, Lock (34) has written an estimate for the damping λ_e due to eddy currents, converted here to a SI value for α:

$$\alpha_{eddy} = \frac{\mu_0 \omega_M t_F^2}{12\rho} \tag{4.26}$$

where t_F designates the ferromagnetic layer thickness. For Fe, with large M_s and small ρ, the eddy current damping is relatively more important than that of Py, forming a sizable fraction of its bulk damping at $t_F = 50$ nm. Py is much less sensitive (35). For films much thinner than the (magnetic) skin depth, eddy-current damping became insignificant, and it became possible to extract α directly from Eq. (4.25) starting in the late 1960s (36). The experimental program of Heinrich has centered on extraction of α in ultrathin epitaxial films (37,38).

4.2.3 Tabulated Materials Parameters

The materials parameters that should be used in the LLG are reasonably well known in the bulk for elemental solids and typical soft alloys at room temperature. Finite-size effects (thickness dependence) remain under investigation, particularly for the damping α. We show parameters for ferromagnetic metals in the "bulk" in Table 4.1. Tabulated dynamics parameters have been measured by FMR, which remains the most quantitative of magnetization dynamics techniques. Values of $\mu_0 M_s$ and g_{eff} come from magnetometry and are confirmed by magnetomechanical experiments, respectively.

4.2.3.1 Bulk Values *Magnetic Moments* Saturation magnetizations M_s were tabulated by Stearns in the Landolt–Börnstein tables (14), reproduced here for 300 K (for the elemental solids Fe, Co, and Ni, the values given here for 300 K have been extrapolated from the 286.5 K values cited using factors of $1 - c\Delta T$, where $c_{Fe} = 1.2 \times 10^{-4} K^{-1}$, $c_{Co} = 5.9 \times 10^{-5} K^{-1}$, and $c_{Ni} = -4.2 \times 10^{-4} K^{-1}$. Values are taken for Fe[1 1 0], Co[0 0 0 1], Ni[1 1 1]; nonnegligible anisotropy in $\mu_0 M_s$ exists, to 0.5% in Co at zero temperature, on the order of 5×10^{-4} in the cubic solids). The alloy values are less certain. For nominal $Ni_{81}Fe_{19}$ alloys, fits to FMR data have indicated a range of 0.95–1.07 T. Interpolation of the Ni, Fe values in Table 4.1 would yield an estimate of 0.91 T with a sensitivity to composition of 0.015 T/%. For constant alloy sputtering target composition (nominal film composition), even though the exiting flux from the target is thought to converge to the internal composition, deposited compositions can vary by several percent, as shown, for example, in the Ni–Ti system (39), due to differences in thermalization of the ejected atoms.

Gyromagnetic Ratios Gyromagnetic ratios are known from a combination of magnetomechanical measurements (g') and FMR measurements (g), taken on bulk samples, in some cases on the same bulk samples (12); in careful experiments, good

agreement (to better than 0.7% error) is found between the measurements satisfying the relationship $1/g' + 1/g = 1$ (40). The error cited for each material is the error for the composition, typically <1%; fits to binary alloy series should improve the error. Later investigations confirmed these values (13). Taking g_{eff} as a free parameter, allowed to range much outside of the band of values listed, or allowed to vary with thickness, can be error-prone.

Damping The most structure-sensitive of the parameters is the damping α, but only in a particular sense. The values given here are α_0, the lowest values found in the literature for variable-frequency FMR spanning linewidth variations significantly greater than the inhomogeneous broadening; see Section 2.2. The Fe value of $\lambda/G = 57$ MHz ($\alpha = 0.0018$) is equal in sputtered films (16) and single-crystal whiskers (15) at room temperature in measurements up to 90 GHz. Ni also shows $\lambda/G = 220$ MHz ($\alpha = 0.023$) equally in the two measurements (18). Co has not been shown to fit the Rado–Ament analysis for whiskers. Measurements of nominally FCC films on MgO have shown different Gilbert damping parameters α for two different crystal directions, not expected for a cubic material.

A higher value of α_{eff} is often obtained for imperfect materials. However, α_{eff} is not expected to be constant with frequency: where damping is increased due to magnetic inhomogeneities (ΔH_0), effective $\alpha_{eff}(\omega)$ is a decreasing function of frequency, converging toward α_0; see Ref. 35 ($\alpha \neq \alpha_0$ thus reflects some departure from a single-domain model). Complicating the matter further is that the lowest values of α have been observed in sputtered films; crystallographically optimized Fe films made by molecular-beam epitaxy (MBE) exhibit significantly higher values of α (41), attributed to the presence of vacancies (38).

4.2.3.2 Finite-Size Effects *Effective Magnetization* There is some question whether the bulk magnetization applies for ultrathin films. Experiments on epitaxial Co/Cu report, in roughly equal numbers, enhanced, reduced, or unchanged magnetic moment μ_B per Co interface *atom*; see Table 21 in Ref. 42. In magnetization dynamics experiments, possible finite-size effects on magnetization are overwhelmed by *surface anisotropy*, proposed by Néel in the 1950s (43). Surface anisotropy introduces free energy terms per unit area of the top and bottom ferromagnetic interfaces as $U_{i,area} = -\sigma_i m_x^2$, where the interfaces favor in-plane magnetization for $\sigma < 0$. Thus,

$$\mathbf{H_{eff}} = 2\frac{\sigma_{top} + \sigma_{bottom}}{\mu_0 M_s}\frac{1}{t_{FM}} m_x \hat{\mathbf{x}}, \quad \mu_0 M_s^{eff} = \mu_0 M_s - \frac{4\sigma}{M_s}\frac{1}{t_{FM}}, \tag{4.27}$$

which, as can be seen, has the sole effect of changing the effective $\mu_0 M_s$ resulting from a fit of the form of Eq. (4.22). First identifications of surface anisotropy in FMR experiments date from the 1970s, although film preparation is in question for experiments from this era. The Permalloy–air interface was found to have a surface anisotropy of $\sigma = 0.08$ mJ/m^2 (44). More recently, Rantschler et al. have estimated σ in Permalloy–Cu, Permalloy–Ag, Permalloy–Ta, finding 0.100, 0.100, and 0.070 mJ/m^2, respectively (45). The positive surface anisotropy, which favors perpendicular magnetization, has the effect of *reducing* the resonance frequencies as if $\mu_0 M_s$ were reduced. In a Cu/Permalloy (5 nm)/Cu film, $\mu_0 M_s^{eff}$ becomes reduced by roughly 0.1 T.

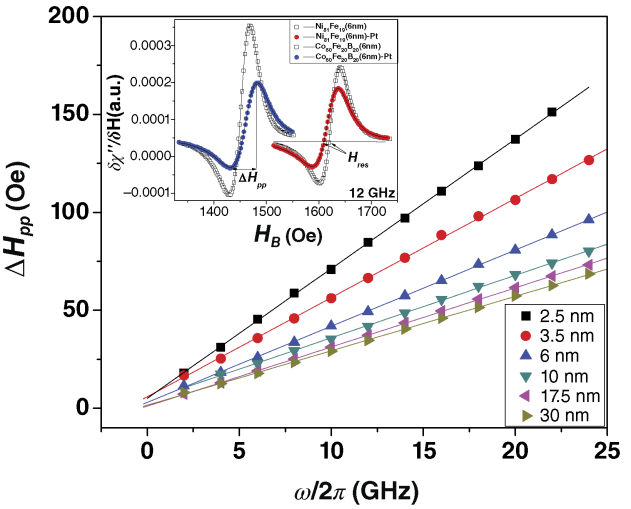

Figure 4.1 Illustration of damping size effect: FMR linewidth ΔH_{pp} as a function of frequency $\omega/2\pi$ for $Ni_{81}Fe_{19}$ (t_{FM}) with Cu (3 nm)/Pt (3 nm) overlayers. There is an inverse dependence of α on the t_{FM} as shown in the slope of the curve. *Inset:* Experimental trace of absorption derivative $\partial\chi''/\partial H$.

Gyromagnetic Ratio It is not clear whether there is a size effect in the gyromagnetic ratio. Some have proposed that the ratio of orbital to spin moment μ_L/μ_S could be enhanced in structures of finite dimension (46), making larger values of g_{eff} plausible in ultrathin films. Variable-frequency, perpendicular FMR (normal condition) is best suited to determine g_{eff} since it enables its isolation from the slope $\Delta H_{res}/\Delta\omega$. Identifications of a size effect in g_{eff} have relied on in-plane FMR (47) or pulsed inductive microwave magnetometry (PIMM) (48), where (at low frequency) $\nu^2 \propto g_{eff}^2 M_s^{eff}$; values of g_{eff} as high as 2.6 were extracted for the Co (3 nm)–Cu system, but with $\mu_0 M_s$ correspondingly lower than that given in Table 4.1 (see Fig. 4.1).

Damping α There is good evidence that the damping α itself exhibits a size effect, where $\alpha = \alpha_0 + Kt^n$. In structures with "spin sinks" in proximity to the FM layer, either heavy elements such as Pt or other FM layers, *spin pumping* can increase α by a factor of roughly 2 over bulk values at thicknesses between 2–5 nm, with inverse dependence on FM thickness ($n = -1$). A detailed review of experiments and theory to 2004 was given by Tserkovnyak et al. (49). However, even in structures without a spin-sink layer, a similar size effect in damping is present. The origin of this size effect is not known.

4.2.4 Pulsed Magnetization Dynamics

Equation (4.20), derived under the assumption of small amplitudes, $\alpha \ll 1$, and sinusoidal driving fields, can be rewritten for arbitrary transverse external fields $H_y(t)$:

$$\ddot{m}_y + \eta\dot{m}_y + \omega_0^2 m_y = (\omega_M + \omega_H)\mu_0\gamma H_y(t), \tag{4.28}$$

where the longitudinal field $\mu_0 H'_{b,z} = \omega_H/|\gamma|$ is taken to be constant. For a step function in transverse magnetic field, the magnetization trajectory describes a damped sinusoid with initial conditions dependent on the initial state. The simplest case is where a finite rotation, in-plane angle $\theta_0 \approx m_{y0} = m_y{}^y(t = 0)$, relaxes to zero after removal of a finite-width, fast fall-time pulse (falling step). The solution for Eq. (4.28) is

$$m_y(t) = m_{y0} e^{-t/\tau} \cos \omega_0 t, \quad \tau = \frac{2}{\eta}, \tag{4.29}$$

where η and ω (both field-dependent) are given as in Eq. (4.21). It is less straightforward to incorporate inhomogeneous broadening in this expression; one can calculate a frequency linewidth by multiplying $\Delta H(\omega)$ by $\partial\omega_0/\partial H$, which can be substituted in the expression for η.

The first high-speed inductive measurements of magnetization dynamics were carried out at IBM-Zurich in the early 1960s (50); the 350 ps rise time of the pulse was sufficient to look at low-frequency precessional dynamics (~1 GHz). The NIST-Boulder group updated the technique using electronics with higher frequency capability (51), and have investigated precessional dynamics up to 3 GHz (52). Pump-probe magneto-optical Kerr effect measurements of small-angle magnetization dynamics, demonstrated first on EuS films (53), were extended to metallic ferromagnetic systems (3), also by the NIST-Boulder group. Similar experiments have been carried out on lithographically defined micrometer-size structures, monitored through time-dependent magnetoresistance (54).

4.3 LARGE-ANGLE DYNAMICS: SWITCHING

In this section, we consider the limit of motions of up to 180°. In Section 4.3.1, we develop a model for the quasistatic switching of a single domain with arbitrary in-plane anisotropy axis. We show that a critical field exists for spontaneous switching at any temperature, with an energy barrier for lower fields. In Section 4.3.2, we develop a simple model for thermal reversal rates over the barrier. Thermally activated switching is relevant for the small patterned elements used in MRAM and is essential in some switching schemes. Finally, in Section 4.3.3, we show integrated switching trajectories for single-domain thin film elements and illustrate the effect of damping α.

4.3.1 Quasistatic Limit: Stoner–Wohlfarth Model

In this section, we consider the quasistatic switching behavior of a single-domain magnetic particle with well-defined anisotropy. Note that any behavior discussed here can be described, in greater detail, through direct integration of the LLG equation. The LLG equation reaches equilibrium $\dot{\mathbf{m}} = 0$, where the precessional term is zero. Thus, the torque

$$\tau = \mathbf{m} \times \mathbf{H}_{\mathbf{eff}} = 0 \tag{4.30}$$

or, equivalently, magnetization $\mathbf{m}$ and applied effective field $\mathbf{H}_{\mathbf{eff}}$ are collinear. This is a useful property in simulation: micromagnetic ground states (for N particles coupled

through magnetostatics or otherwise) can be found by integrating the LLG forward to convergence, accelerated by taking unphysically large values of α.

Energy Expression We assume that the particle has some built-in structure, or *anisotropy*, which favors magnetization in a particular direction. This model was first considered by Stoner and Wohlfarth in 1948 (55). The anisotropy can be expressed as a contribution to the energy U_A, which depends on the magnetization orientation ϕ,

$$U_A(\phi) = K_u \sin^2(\phi - \phi_u), \tag{4.31}$$

where ϕ_u is the angle of the preferred direction of the magnetization. The energy is minimized where $\phi = \phi_u$ and maximized where $\phi = \phi_u \pm (\pi/2)$ (hard axis), but is equivalent for $\phi = \phi_u$ and $\phi = \phi_u \pm \pi$ (easy axis). The anisotropy axis thus has no direction, only an orientation. K_u is an anisotropy constant and takes units of erg/cm^3 in cgs units or J/m^3 in SI units.

With the definitions

$$H_K \equiv \frac{2K_u}{M_s}, \quad h_b = \frac{H_b}{H_K}, \quad u = \frac{U}{M_s H_K}, \tag{4.32}$$

the normalized total energy including Zeeman and anisotropy terms is

$$u = -m_z h_b + \frac{1}{4}\left[1 - \cos 2\phi \cos 2\phi_u + \sin 2\phi \sin 2\phi_u\right]. \tag{4.33}$$

Hard and Easy Axes Magnetization In the hard axis case, $\phi_u = (\pi/2)$; in the easy axis case, $\phi_u = 0$. For these two cases, Eq. (4.33) becomes

$$u_{HA} = -m_z h_b + \frac{1}{2} m_z^2, \quad u_{EA} = -m_z h_b + \frac{1}{2}\left(1 - m_z^2\right), \tag{4.34}$$

since $m_z = \cos\phi$. We can find the equilibrium magnetization by taking the first derivative of u with respect to m_z, and find

$$m_z^{HA} = h_b, \quad m_z^{EA} = -h_b, \tag{4.35}$$

which is a stable minimum only for the hard axis case. The energy minimum for the easy axis case must lie on either extremum, $\phi = 0$ or $\phi = \pi$. Clearly, the lowest energy is found for $\phi = 0$ for $h_Z > 0$ and $\phi = \pi$ for $h_Z < 0$.

Switching does not respond simply to the energy minimum. For an initial state $\phi = \pi$ under the application of $0 < h_z < 1$, or $H_b < H_K$, the $\phi = 0$ state becomes lower and lower in energy compared with the $\phi = \pi$ state, but the single domain cannot rotate into it. As illustrated in Fig. 4.2, an energy barrier develops between the two states. Small excursions away from $\varphi = \pi$ only raise the energy. Only when the condition $du/d\phi < 0$ is fulfilled over the whole domain $-1 < h_b < 1$ will the particle switch. This condition becomes true for $h_b \geq 1$ or $H_b > H_K$. For lower fields, thermal activation is required to climb the energy barrier.

General Case: The Switching Astroid Richer behavior emerges if we consider the problem more generally. We would like to consider the critical field

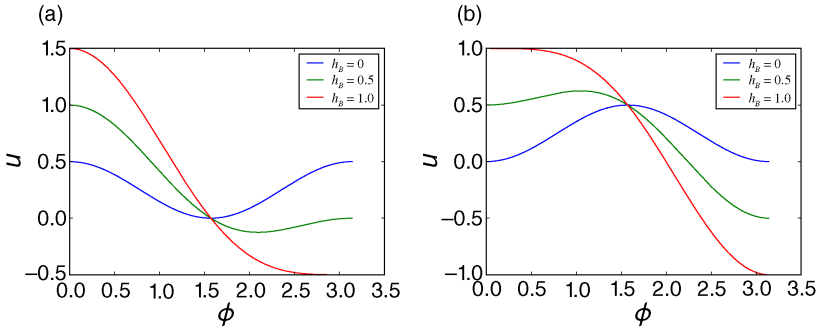

Figure 4.2 Energy landscapes: hard axis (a) and easy axis (b). Note the metastable equilibria at $\phi = \pi$ for the easy axis case if $H_b < 1$. Angles in radians.

for switching h_0. We now allow both the reduced magnetization $\mathbf{m} = \mathbf{M}/M_s$ and the reduced field $\mathbf{h} = \mathbf{H}/H_K$ to take any direction in the x–y plane. We will see that the critical field is a function of angle as well as magnitude, so $\mathbf{h_0}$ is a dividing line in the control plane. Here we follow Thiaville's notation (56). A convenient aspect of this formulation is that it can be used for any form of the in-plane anisotropy energy, given here as $G(\phi)$. The magnetization takes angle ϕ with respect to the x-axis, giving us magnetization vector $\mathbf{m}$ and its orthogonal in-plane vector $\hat{\mathbf{e}} \equiv \hat{\phi}$; this is a different coordinate system than the y–z film plane considered up until now.

$$\mathbf{m}(\phi) = \cos\phi\,\hat{\mathbf{x}} + \sin\phi\,\hat{\mathbf{y}}, \qquad \hat{\phi} = \hat{\mathbf{e}} = -\sin\phi\,\hat{\mathbf{x}} + \cos\phi\,\hat{\mathbf{y}}, \tag{4.36}$$

$$\frac{\partial \mathbf{m}(\phi)}{\partial \phi} = \hat{\mathbf{e}}, \qquad \frac{\partial^2 \mathbf{m}(\phi)}{\partial \phi^2} = -\mathbf{m}. \tag{4.37}$$

To find equilibria, we already know to take

$$\frac{\partial[-\mathbf{m}(\phi)\cdot\mathbf{h_0} + u_A(\phi)]}{\partial\phi} = -\hat{\mathbf{e}}\cdot\mathbf{h_0} + \frac{\partial u_A(\phi)}{\partial\phi} = 0 \tag{4.38}$$

and for stability, $\frac{\partial^2 u}{\partial \phi^2} = 0$.

$$\frac{\partial\left[-\hat{\mathbf{e}}\cdot\mathbf{h}_0 + (\partial u_A(\phi))/\partial\phi\right]}{\partial\phi} = \mathbf{m}\cdot\mathbf{h}_0 + \frac{\partial^2 u_A(\phi)}{\partial\phi^2} = 0. \tag{4.39}$$

After decomposing $\mathbf{h_0} = h_0^m\mathbf{m} + h_0^e\mathbf{e}$, these two criteria give

$$\mathbf{h_0} = -\frac{\partial^2 u_A(\phi)}{\partial\phi^2}\mathbf{m} + \frac{\partial u_A(\phi)}{\partial\phi}\hat{\mathbf{e}} = -G''\mathbf{m} + G'\hat{\mathbf{e}}. \tag{4.40}$$

From here, we can transfer back into the Cartesian system using Eqs. (4.36 and 4.37,

$$\mathbf{h_0} = -(G''\cos\phi + G'\sin\phi)\hat{\mathbf{x}} + (-G''\sin\phi + G'\cos\phi)\hat{\mathbf{y}}. \tag{4.41}$$

If we fix $\hat{\mathbf{x}}$ for the uniaxial anisotropy easy axis, after some algebra, this yields

$$\mathbf{h_0} = -\cos^3\phi\,\hat{\mathbf{x}} + \sin^3\phi\,\hat{\mathbf{y}}. \tag{4.42}$$

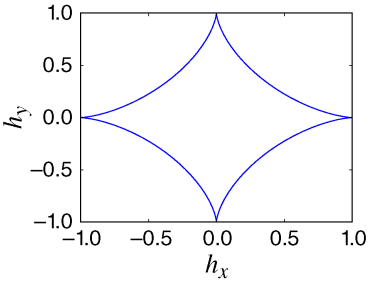

Figure 4.3 The switching astroid described by Eq. (4.42). Magnetization does not become destabilized until the field |h| lies outside the boundary.

For $\phi = 0$ ($m = 1$) and $\phi = \pi$ ($m = -1$), the magnetization lies along the easy axis. In order to destabilize the positive (negative) magnetization $m = \pm 1$, it is necessary to apply an opposite, negative (positive) field $H = \mp H_K$, or $h = \mp 1$. The boundary between switching and no switching, known as the *switching astroid*, is shown in Fig. 4.3.

4.3.2 Thermally Activated Switching

For easy axis switching, we saw that for applied fields large enough, $h > -m$, there is no energy barrier for reversal. Magnetization reversal is continuously energetically favored for rotation of $\mathbf{m}$ away from $\varphi = 0$. For smaller, subcritical fields $|h| < 1$ directed along the easy axis, an energy barrier exists for switching, as shown in Fig. 4.2. If no thermal energy were available, a particle would never switch for $|h| < 1$. Thermal fluctuations help drive the magnetization over the barrier, and yield a finite, thermally activated switching rate that depends on the applied field and volume of the particle.

In Eq. (4.34), if we take our starting point as $m_z = 1$ ($\phi = 0$) and apply a field h along $-\hat{\mathbf{z}}$ (opposite to the magnetization direction), we find that the energy difference between the initial state and the unstable equilibrium at $m_z = -h$ is

$$\Delta u = u_{eq} - u(\varphi = 0), \quad \Delta u = \frac{1}{2}(1 - h_b)^2. \tag{4.43}$$

The Arrhenius–Néel equation for kinetics (57) states that the frequency ν of overcoming the barrier (and switching) is

$$\nu(\Delta U, V, T) = \nu_0 e^{-\Delta E_b / k_B T}, \quad \Delta E_b = \frac{1}{2} M_s H_K V \left(1 - \frac{H_b}{H_K}\right)^n, \quad n = 2 \tag{4.44}$$

for an energy barrier ΔE_b. Here k_B is the Boltzmann constant, $k_B(300\ \mathrm{K}) = 25.86$ meV, and ν_0 is a temperature-independent attempt frequency. The value $n = 2$ obtains for easy axis switching; for the full Stoner–Wohlfarth model with arbitrary orientation of the anisotropy axes (not shown here), $1.5 \leq n \leq 2$. With a characteristic time $\tau = \nu^{-1}$, if a switching experiment is carried out many times, the number of times N the particle does *not* reverse in time t is given by

$$\frac{\partial N}{\partial t} = -\frac{N}{\tau}, \quad N(t) = N_0 e^{-t/\tau} \tag{4.45}$$

for N_0 attempts. The probability $P_s(t)$ for switching after time t is thus

$$P_s(t) = 1 - P_{ns}(t) = 1 - e^{-t/\tau}, \quad \tau = \nu_0^{-1} e^{\Delta E_b / k_B T}, \tag{4.46}$$

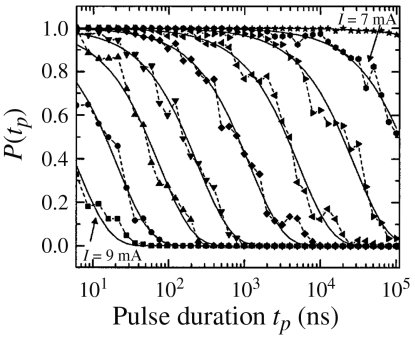

Figure 4.4 Probability $P(t_p)$ of not-switching a magnetic tunnel junction in response to field pulses of width t_p and variable pulse amplitude I. (Reproduced from Ref. 59 with permission from AIP Publishing LLC.)

where ΔE_b was given in Eq. (4.44). Wernsdorfer et al. (58) applied Eq. (4.46) to the low-temperature (0.2–6 K) and low-speed switching of a single 25 nm diameter Co nanoparticle, measured using a SQUID microbridge with temporal resolution of ~250 μs.

Thermal Switching Experiments: MRAM In the context of MRAM, Rizzo and coworkers at Motorola applied Eq. (4.46), $n = 2$, to the thermal switching in magnetic tunnel junctions (59) for pulse durations t_p of 5 ns to 100 μs at room temperature. The magnetic state was characterized through the magnetoresistance. Data are shown in Fig. 4.4 for the probability of not-switching after pulse duration t_p $P_{ns}(t_p)$ under the application of field pulses with different values (currents) of H/H_K (given there as i/i_{sw}). Excellent agreement is shown with the single-domain/single-energy-barrier model. Other contemporaneous experiments showed more complicated behavior, with multiple energy barriers indicating thermal activation of domain walls (60). Further experiments characterized the full thermal switching astroid, with arbitrary pulse direction, at constant sweep rate (61).

4.3.3 Switching Trajectory

In this section we will examine a calculated trajectory for switching of a thin-film element. A convenient dimensionless form can be used for integration if we take out a factor $T = \mu_0 \gamma M_s$. We define a dimensionless $t' = T \cdot t$,

$$T^{-1}\begin{bmatrix}\dot{\theta}\\ \dot{\phi}\end{bmatrix} = \begin{bmatrix}\partial\theta/\partial t'\\ \partial\phi/\partial t'\end{bmatrix} = \frac{1}{1+\alpha^2}\begin{bmatrix}\alpha & 1\\ -1/\sin\theta & \alpha/\sin\theta\end{bmatrix}\begin{bmatrix}h_\theta^{eff}\\ h_\phi^{eff}\end{bmatrix}. \tag{4.47}$$

Note that for Permalloy, for example, $t' = 1$ is reached for $t = 64.5$ ps. Fields can be transferred from the rotating frame to the Cartesian frame through

$$\begin{bmatrix}h_\theta\\ h_\phi\end{bmatrix} = \begin{bmatrix}\cos\theta\cos\phi & \cos\theta\sin\phi & -\sin\theta\\ -\sin\phi & \cos\phi & 0\end{bmatrix}\cdot\begin{bmatrix}h_x\\ h_y\\ h_z\end{bmatrix}. \tag{4.48}$$

Example: Influence of α For a useful example, we can take a thin film magnetized in plane, evolving under the influence of an in-plane switching field. To

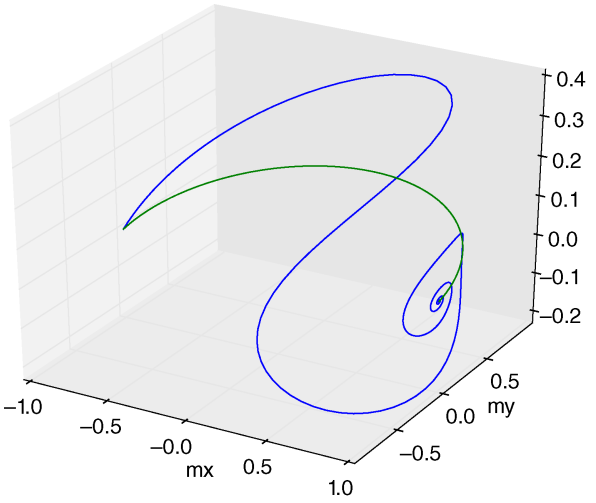

Figure 4.5 Switching on the unit sphere (phase plot, time is implicit) under the influence of $h = +1$, initial condition $m_x = -1$, thin film magnetized in the x–y film plane. The z-axis is taken to be the film normal. Trajectories for $\alpha = 1$ and $\alpha = 0.1$ are shown. Total integration time is $t' = 100$, or ~6 ns

be consistent with the form where the polar axis is $\hat{\mathbf{z}}$, the film plane is x–y, and we have effective fields as follows:

$$h_x = h_b. \quad h_z = -\cos\theta \tag{4.49}$$

$$\begin{bmatrix} h_\theta \\ h_\phi \end{bmatrix} = \begin{bmatrix} h_b \cos\theta\cos\phi + \sin\theta\cos\theta \\ -h_b \sin\phi \end{bmatrix}. \tag{4.50}$$

The expression for direct integration is then given as

$$\begin{bmatrix} \partial\theta/\partial t' \\ \partial\phi/\partial t' \end{bmatrix} = \frac{1}{1+\alpha^2}\begin{bmatrix} \alpha & 1 \\ -1/\sin\theta & \alpha/\sin\theta \end{bmatrix}\begin{bmatrix} h_b\cos\theta\cos\phi + \sin\theta\cos\theta \\ -h_b\sin\phi \end{bmatrix}. \tag{4.51}$$

We show integrated trajectories from $m_x = -1$ to $m_x = +1$ in Fig. 4.5. Notice the influence of α on the convergence toward a new equilibrium direction, very rapid for $\alpha = 1$, and less direct for $\alpha = 0.1$. The effective field from demagnetization keeps the magnetization trajectory more in-plane than out-of-plane.

4.4 MAGNETIZATION SWITCHING BY SPIN-TRANSFER

In this final section, we show how spin-torque terms are added to the LLG equation (Section 4.4.1), write the full LLG equation with spin-torque terms (Section 4.4.2), and show a simple estimate for the spin-torque switching current. Sun has presented a thorough set of calculations of spin-torque switching for single domains, with anisotropy and thermal activation (62).

4.4.1 Additional Terms to the LLG

Spin-polarized currents can act as an additional source for torque on the magnetization (63,64). A spin-polarized electron carries an angular momentum $\hbar$. If the electron is

scattered in the FM layer, reversing its spin through transfer of angular momentum to $\mathbf{m}$, $\mathbf{m}$ rotates according to the torque exerted. This is *spin-transfer torque*. The angular momentum transferred per unit time (torque) is thus $\tau \sim \hbar JSP/(2e)$, where J is the current density, e is the electronic charge, $0 < P < 1$ is the spin polarization, and S is the area. Taking $\hat{\mathbf{p}}$ as the *spin* direction of the spin-polarized current incident on the FM (i.e., the direction of $\mathbf{m_2}$ if current is injected from $\mathbf{m_2}$ into $\mathbf{m_1}$), we have for the additional term to magnetization dynamics, through Eq. (4.15).

$$\dot{\mathbf{m}}_{STT} = -\frac{|\gamma|}{St\mu_0 M_s}\boldsymbol{\tau} = -\frac{\hbar J|\gamma|P}{2e\mu_0 M_s t}\hat{\mathbf{p}}. \tag{4.52}$$

Most interesting to note here is that there can be a contribution to magnetization dynamics only where $\mathbf{m}$ and $\mathbf{p}$ form angles other than zero and π. Any components of $\dot{\mathbf{m}}_{STT}$ that are parallel to $\mathbf{m}$ will make no contribution, since torque terms can only rotate the magnetization, $\dot{\mathbf{m}} \cdot \mathbf{m} = 0$. The transverse component of the spin current can be isolated by taking $\mathbf{m} \times \mathbf{m} \times \mathbf{p}$ and the contribution to magnetization dynamics given by spin-torque is

$$\dot{\mathbf{m}} = \cdots + \gamma A_J\, \mathbf{m} \times \mathbf{m} \times \mathbf{p} + \gamma B_J\, \mathbf{m} \times \mathbf{p}, \quad A_J \equiv A \approx \frac{\hbar P}{2e\mu_0 M_s t} J, \tag{4.53}$$

where A_J is the *Slonczewski* spin-torque. A_J is an experimental parameter, proportional to (an odd function of) current density J, with estimate as given. B_J is the *field-like* spin-torque, introduced separately; its dependence on current and voltage is under investigation (65,66). Both terms have units of field (T).

4.4.2 Full-Angle LLG with Spin-Torque

In terms of the magnetization coordinates, Eq. (4.52) can be expressed as

$$\dot{\mathbf{m}} = \cdots + \gamma A_J\, \hat{\mathbf{m}} \times \hat{\mathbf{m}} \times \left(p_\theta \hat{\boldsymbol{\theta}} + p_\phi \hat{\boldsymbol{\phi}}\right) + \gamma B_J\, \hat{\mathbf{m}} \times \left(p_\theta \hat{\boldsymbol{\theta}} + p_\phi \hat{\boldsymbol{\phi}}\right). \tag{4.54}$$

Defining $T = \gamma\mu_0 M_s$, normalized time $t' = T \cdot t$, and normalized spin-torque parameters $A'_J = A_J/M_s$, $B'_J = B_J/M_s$, the single-particle, full-angle LLG with spin-torque can be written as

$$T^{-1}\begin{bmatrix}\dot{\theta}\\ \dot{\phi}\end{bmatrix} = \frac{1}{1+\alpha^2}\begin{bmatrix}\alpha & 1\\ -1/\sin\theta & \alpha/\sin\theta\end{bmatrix}\begin{bmatrix}h_\theta^{eff}\\ h_\phi^{eff}\end{bmatrix} + \frac{1}{1+\alpha^2}\begin{bmatrix}-A'_J - \alpha B'_J & \alpha A'_J - B'_J\\ \left(B'_J - \alpha A'_J\right)/\sin\theta & \left(-A'_J - \alpha B'_J\right)/\sin\theta\end{bmatrix}\begin{bmatrix}p_\theta\\ p_\phi\end{bmatrix}.$$

Nulling of Damping If the effective field and the injected spin polarization, $\mathbf{H}$ and $\hat{\mathbf{p}}$, are collinear, the effective damping can be made zero through the spin-torque. Damping is expressed in the on-diagonal terms of the right-hand-side of the equation. These cancel in the case of

$$A_J \geq \alpha H. \tag{4.56}$$

Since it is known that A_J is proportional to current, we can express

$$A_J = AJ \geq \alpha H, \quad J \geq \frac{\alpha H}{A}. \tag{4.57}$$

Zero damping implies that equilibrium magnetization becomes unstable to any perturbation. A remarkable result of the nonlinear aspects of the LLG is that a limit cycle, oscillating around the equilibrium, can replace the stable state. The stable precession is the basis of the spin-torque oscillator, a microwave power source driven by dc currents.

For higher values of current density J, the limit cycle becomes destabilized, replaced by stable equilibrium π away. This is *spin-torque switching*. Equation (4.5) suggests that lower current (lower-power) spin-torque switching is favored by materials with lower values of damping α.

Interested readers may refer to Ref. 38 for more details on the physical basis of ferromagnetic relaxation, Ref. 67 on magnetic anisotropies in ultrathin films, Ref. 68 on electrical measurements of magnetization dynamics in submicrometer structures, Ref. 69 on spin-transfer torque, and Ref. 70 on nonlinear magnetization dynamics in nanosystems.

ACKNOWLEDGMENTS

I thank the National Science Foundation (NSF-ECCS 0925829) and *Fondation Nanosciences* for support as well as SPINTEC for hospitality during the preparation of this chapter.

REFERENCES

1. L. Landau and E. Lifshitz, "On the theory of the dispersion of magnetic permeability in ferromagnetic bodies," *Phys. Zeitsch. Sowjet.* **8**, pp. 153–169 (1935). Reprinted and translated as *Ukr. J. Phys.* **53**, pp. 14–22 (2008).
2. H. Brooks, "Ferromagnetic anisotropy and the itinerant electron model," *Phys. Rev.* **58**, pp. 909–918 (1940); doi: 10.1103/PhysRev.58.909.
3. T. Crawford, T. Silva, C. Teplin, and C. Rogers, "Subnanosecond magnetization dynamics measured by the second-harmonic magneto-optic Kerr effect," *Appl. Phys. Lett.* **74**, pp. 3386–3388 (1999); doi: 10.1063/1.123353.
4. R. Liboff, *Introduction to Quantum Mechanics*, vol. 4, Addison-Wesley, Boston, MA, 2002.
5. A. Einstein and W. De Haas, "Experimental proof of Ampere's molecular currents," *Verh. Dtsch. Phys. Ges.* **17**, pp. 152–170 (1915).
6. V. Y. Frenkel, "On the history of the Einstein–de Haas effect," *Sov. Phys. Usp.* **22**, pp. 580–584 (1979); doi: 10.1070/PU1979v022n07ABEH005587.
7. S. J. Barnett, "Magnetization by rotation," *Phys. Rev.* **6**, pp. 239–270 (1915); doi: 10.1103/PhysRev.6.239.
8. S. Barnett and G. Kenny, "Gyromagnetic ratios of iron, cobalt and many binary alloys of iron, cobalt and nickel," *Phys. Rev.* **87**, pp. 723–734 (1952); doi: 10.1103/PhysRev.87.723.
9. T. L. Gilbert and J. M. Kelly,"Anomalous rotational damping in ferromagnetic sheets," in *Conference on Magnetism and Magnetic Materials*, Pittsburgh, PA, June 14–16, 1955, American Institute of Electrical Engineers, New York, October 1955, pp. 253–263.

10. T. Gilbert, "A phenomenological theory of damping in ferromagnetic materials," *IEEE Trans. Magn.* **40**, pp. 3443–3449 (2004); doi: 10.1109/TMAG.2004.836740.
11. W. Saslow, "Landau–Lifshitz or Gilbert damping? That is the question," *J. Appl. Phys.* **105**, 07D315 (2009); doi: 10.1063/1.3077204.
12. A. Meyer and G. Asch, "Experimental g' and g values of Fe, Co, Ni and their alloys," *J. Appl. Phys.* **32**, pp. 330–333 (1961); doi: 10.1063/1.2000457.
13. R. A. Reck and D. L. Fry, "Orbital and spin magnetization in Fe-Co, Fe-Ni, and Ni-Co," *Phys. Rev.* **184**, pp. 492–495, (1969); doi: 10.1103/PhysRev.184.492.
14. Landolt–Börnstein Tables, Chapter III-13: Metals: Phonon States, Electron States, and Fermi Surfaces, Springer, Berlin, 1990, pp. 100–101.
15. Z. Frait and D. Fraitova, "Ferromagnetic resonance and surface anisotropy in iron single crystals," *J. Magn. Magn. Mater.* **15–18**, (Part 2), pp. 1081–1082 (1980); doi: 10.1016/0304-8853(80)90895-1.
16. F. Schreiber, J. Pflaum, Z. Frait, Th. Mühge, and J. Pelzl, "Gilbert damping and g-factor in Fe_xCo_{1-x} alloy films," *Solid State Commun.* **93**, pp. 965–968 (1995); doi: 10.1016/0038-1098(94)00906-6.
17. C. Scheck, L. Cheng, I. Barsukov, Z. Frait, and W. Bailey, "Low relaxation rate in epitaxial vanadium-doped ultrathin iron films," *Phys. Rev. Lett.* **98**, 117601 (2007); doi: 10.1103/PhysRevLett.98.117601.
18. S. Bhagat and P. Lubitz, "Temperature dependence of ferromagnetic relaxation in the 3d transition metals," *Phys. Rev. B* **10**, pp. 179–185 (1974); doi: 10.1103/PhysRevB.10.179.
19. Y. Guan and W. E. Bailey, "Ferromagnetic relaxation in $(Ni_{81}Fe_{19})_{1-x}Cu_x$ thin films: band filling at high Z," *J. Appl. Phys.* **101**, 09D104 (2007); doi: 10.1063/1.2709750.
20. A. Ghosh, J. F. Sierra, S. Auffret, U. Ebels, and W. E. Bailey, "Dependence of nonlocal Gilbert damping on the ferromagnetic layer type in ferromagnet/Cu/Pt heterostructures," *Appl. Phys. Lett.* **98**, 052508 (2011); doi: 10.1063/1.3551729.
21. Y. Li and W. E. Bailey, "Wave-number-dependent Gilbert damping in metallic ferromagnets," *Phys. Rev. Lett.* **116**, 117602 (2014); doi: 10.1103/PhysRevLett.116.117602.
22. C. Bilzer, T. Devolder, J.-V. Kim, G. Counil, C. Chappert, S. Cardoso, and P. P. Freitas, "Study of the dynamic magnetic properties of soft CoFeB films," *J. Appl. Phys.* **100**, 053903 (2006); doi: 10.1063/1.2337165.
23. N. Chan, V. Kambersky, and D. Fraitova, "Impedance matrix of thin metallic ferromagnetic films and SSWR in parallel configuration," *J. Magn. Magn. Mater.* **214**, pp. 93–98 (2000); doi: 10.1016/S0304-8853(99)00776-3.
24. I. I. Rabi, J. R. Zacharias, S. Millman, and P. Kusch, "A new method of measuring nuclear magnetic moment," *Phys. Rev.* **53**, pp. 318–327 (1938); doi: 10.1103/PhysRev.53.318.
25. P. Forman, "Swords into ploughshares: breaking new ground with radar hardware and technique in physical research after World War II," *Rev. Mod. Phys.* **67**, pp. 397–455 (1995); doi: 10.1103/RevModPhys.67.397.
26. E. Zavoisky, "Paramagnetic relaxation of liquid solutions for perpendicular fields," *J. Phys. USSR*, **9**, pp. 211–216 (1945).
27. E. M. Purcell, H. C. Torrey, and R. V. Pound, "Resonance absorption by nuclear magnetic moments in a solid," *Phys. Rev.* **69**, pp. 37–38 (1946); doi: 10.1103/PhysRev.69.37.
28. J. Griffiths, "Anomalous high-frequency resistance in ferromagnetic metals," *Nature* **158**, pp. 670–671 (1946); doi: 10.1038/158670a0.
29. C. Kittel, "Interpretation of anomalous Larmor frequencies in ferromagnetic resonance experiment," *Phys. Rev.* **71**, pp. 270–271 (1947); doi: 10.1103/PhysRev.71.270.2.
30. R. McMichael and P. Krivosik, "Classical model of extrinsic ferromagnetic resonance linewidth in ultrathin films," *IEEE Trans. Magn.* **40**, pp. 2–11 (2004); doi: 10.1109/TMAG.2003.821564.
31. W. Ament and G. Rado, "Electromagnetic effects of spin wave resonance in ferromagnetic metals," *Phys. Rev.* **97**, pp. 1558–1566 (1955); doi: 10.1103/PhysRev.97.1558.
32. K. Gilmore, Y. U. Idzerda, and M. D. Stiles, "Identification of the dominant precession-damping mechanism in Fe, Co, and Ni by first-principles calculations," *Phys. Rev. Lett.* **99**, 027204 (2007); doi: 10.1103/PhysRevLett.99.027204.
33. M. Fähnle, J. Seib, and C. Illg, "Relating Gilbert damping and ultrafast laser-induced demagnetization," *Phys. Rev. B* **82** 144405 (2010); doi: 10.1103/PhysRevB.82.144405.
34. J. Lock, "Eddy current damping in thin metallic ferromagnetic films," *Br. J. Appl. Phys.* **17**, pp. 1645–1647 (1966); doi: 10.1088/0508-3443/17/12/415.

35. C. Scheck, L. Cheng, and W. Bailey, "Low damping in epitaxial sputtered Fe films," *Appl. Phys. Lett.* **88**, 252510 (2006); doi: 10.1063/1.2216031.
36. C. E. Patton, "Linewidth and relaxation processes for the main resonance in the spin-wave spectra of Ni–Fe alloy films," *J. Appl. Phys.* **39**, pp. 3060–3068 (1968); doi: 10.1063/1.1656733.
37. B. Heinrich, K. Urquhart, A. Arrott, J. Cochran, K. Myrtle, and S. Purcell, "Ferromagnetic-resonance study of ultrathin BCC Fe(1 0 0) films grown epitaxially on FCC Ag(1 0 0) substrates," *Phys. Rev. Lett.* **59**, pp. 1756–1759 (1987); doi: 10.1103/PhysRevLett.59.1756.
38. B. Heinrich, "Spin relaxation in magnetic metallic layers and multilayers," in *Ultrathin Magnetic Structures III: Fundamentals of Nanomagnetism*, eds. J. A. C. Bland and B. Heinrich, Chapter 5, Springer, Berlin, 2005, pp. 143–210; doi: 10.1007/3-540-27163-5_5.
39. M. Bendahan, P. Canet, J.-L. Seguin, and H. Carchano, "Control composition study of sputtered Ni-Ti shape memory alloy film," *Mater. Sci. Eng. B* **34**, pp. 112–115 (1995); doi: 10.1016/0921-5107(95)01237-0.
40. C. Kittel, "On the gyromagnetic ratio and spectroscopic splitting factor of ferromagnetic substances," *Phys. Rev.* **76**, pp. 743–748 (1949); doi: 10.1103/PhysRev.76.743.
41. R. Urban, G. Woltersdorf, and B. Heinrich, "Gilbert damping in single and multilayer ultrathin films: role of interfaces in nonlocal spin dynamics," *Phys. Rev. Lett.* **87**, 217204 (2001); doi: 10.1103/PhysRevLett.87.217204.
42. C. A. F. Vaz, J. A. C. Bland, and G. Lauhoff, "Magnetism in ultrathin film structures," *Rep. Prog. Phys.* **71**, 056501 (2008); doi: 10.1088/0034-4885/71/5/056501.
43. L. Néel, "Anisotropie magnétique superficielle et surstructures d'orientation," *J. Phys. Radium*, **15**, pp. 225–239 (1954); doi: 10.1051/jphysrad:01954001504022500.
44. G. C. Bailey and C. Vittoria, "Presence of magnetic surface anisotropy in Permalloy films," *Phys. Rev. B* **8**, pp. 3247–3251 (1973); doi: 10.1103/PhysRevB.8.3247.
45. J. O. Rantschler, P. J. Chen, A. S. Arrott, R. D. McMichael, J. W. F. Egelhoff, and B. B. Maranville, "Surface anisotropy of Permalloy in NM/NiFe/NM multilayers," *J. Appl. Phys.* **97**, 10J113 (2005); doi: 10.1063/1.1853711.
46. P. Gambardella, S. Rusponi, M. Veronese, S. S. Dhesi, C. Grazioli, A. Dallmeyer, I. Cabria, R. Zeller, P. H. Dederichs, K. Kern, C. Carbone, and H. Brune, "Giant magnetic anisotropy of single cobalt atoms and nanoparticles," *Science* **300**, pp. 1130–1133 (2003); doi: 10.1126/science.1082857.
47. J.-M. Beaujour, J. Lee, A. Kent, K. Krycka, and C.-C. Kao, "Magnetization damping in ultrathin polycrystalline Co films: evidence for nonlocal effects," *Phys. Rev. B* **74**, 214405 (2006); doi: 10.1103/PhysRevB.74.214405.
48. J. P. Nibarger, R. Lopusnik, Z. Celinski, and T. J. Silva, "Variation of magnetization and the Landé *g* factor with thickness in Ni-Fe films," *Appl. Phys. Lett.* **83**, pp. 93–95 (2003); doi: 10.1063/1.1588734.
49. Y. Tserkovnyak, A. Brataas, G. Bauer, and B. Halperin, "Nonlocal magnetization dynamics in ferromagnetic heterostructures," *Rev. Mod. Phys.* **77**, pp. 1375–1421 (2005); doi: 10.1103/RevModPhys.77.1375.
50. P. Wolf, "Free oscillations of the magnetization in Permalloy films," *J. Appl. Phys.* **32**, pp. S95–S96 (1961); doi: 10.1063/1.2000514.
51. T. Silva, C. Lee, T. Crawford, and C. Rogers, "Inductive measurement of ultrafast magnetization dynamics in thin-film Permalloy," *J. Appl. Phys.* **85**, pp. 7849–7862 (1999); doi: 10.1063/1.370596.
52. A. B. Kos, T. J. Silva, and P. Kabos, "Pulsed inductive microwave magnetometer," *Rev. Sci. Instrum.* **73**, pp. 3563–3569 (2002); doi: 10.1063/1.1505657.
53. M. R. Freeman, "Picosecond pulsed-field probes of magnetic systems," *J. Appl. Phys.* **75**, pp. 6194–6198 (1994); doi: 10.1063/1.355454.
54. S. E. Russek, S. Kaka, and M. Donahue, "High-speed dynamics, damping, and relaxation times in submicrometer spin-valve devices," *J. Appl. Phys.* **87**, pp. 7070–7073 (2000); doi: 10.1063/1.372934.
55. E. C. Stoner and E. P. Wohlfarth, "A mechanism of magnetic hysteresis in heterogeneous alloys," *Philos. Trans. R. Soc. A* **240**, pp. 599–642 (1948); doi: 10.1098/rsta.1948.0007.
56. A. Thiaville, "Extensions of the geometric solution of the two-dimensional coherent magnetization rotation model," *J. Magn. Magn. Mater.* **182**, pp. 5–18 (1998); doi: 10.1016/S0304-8853(97)01014-7.
57. L. Néel, "Some theoretical aspects of rock-magnetism," *Adv. Phys.* **4**, pp. 191–243 (1955); doi: 10.1080/00018735500101204.

58. W. Wernsdorfer, E. B. Orozco, K. Hasselbach, A. Benoit, B. Barbara, N. Demoncy, A. Loiseau, H. Pascard, and D. Mailly, "Experimental evidence of the Néel–Brown model of magnetization reversal," *Phys. Rev. Lett.* **78**, pp. 1791–1794 (1997); doi: 10.1103/PhysRevLett.78.1791.
59. N. D. Rizzo, M. DeHerrera, J. Janesky, B. Engel, J. Slaughter, and S. Tehrani, "Thermally activated magnetization reversal in submicron magnetic tunnel junctions for magnetoresistive random access memory," *Appl. Phys. Lett.* **80**, pp. 2335–2337 (2002); doi: 10.1063/1.1462872.
60. R. H. Koch, G. Grinstein, G. A. Keefe, Y. Lu, P. L. Trouilloud, W. J. Gallagher, and S. S. P. Parkin, "Thermally assisted magnetization reversal in submicron-sized magnetic thin films," *Phys. Rev. Lett.* **84**, pp. 5419–5422 (2000); doi: 10.1103/PhysRevLett.84.5419.
61. J. Z. Sun, J. C. Slonczewski, P. L. Trouilloud, D. Abraham, I. Bacchus, W. J. Gallagher, J. Hummel, Y. Lu, G. Wright, S. S. P. Parkin, and R. H. Koch, "Thermal activation-induced sweep-rate dependence of magnetic switching astroid," *Appl. Phys. Lett.* **78**, pp. 4004–4006 (2001); doi: 10.1063/1.1379596.
62. J. Z. Sun, "Spin-current interaction with a monodomain magnetic body: a model study," *Phys. Rev. B* **62**, pp. 570–578 (2000); doi: 10.1103/PhysRevB.62.570.
63. J. Slonczewski, "Current-driven excitation of magnetic multilayers," *J. Magn. Magn. Mater.* **159**, pp. 1–7 (1996); doi: 10.1016/0304-8853(96)00062-5.
64. Y. B. Bazaliy, B. Jones, and S.-C. Zhang, "Modification of the Landau–Lifshitz equation in the presence of a spin-polarized current in colossal- and giant-magnetoresistive materials," *Phys. Rev. B* **57**, pp. R3213–R3216 (1998); doi: 10.1103/PhysRevB.57.R3213.
65. S. Petit, C. Baraduc, C. Thirion, U. Ebels, Y. Liu, M. Li, P. Wang, and B. Dieny, "Spin-torque influence on the high-frequency magnetization fluctuations in magnetic tunnel junctions," *Phys. Rev. Lett.* **98**, 077203 (2007); doi: 10.1103/PhysRevLett.98.077203.
66. S. Petit, N. de Mestier, C. Baraduc, C. Thirion, Y. Liu, M. Li, P. Wang, and B. Dieny, "Influence of spin-transfer torque on thermally activated ferromagnetic resonance excitations in magnetic tunnel junctions," *Phys. Rev. B* **78** 184420 (2008); doi: 10.1103/PhysRevB.78.184420.
67. M. Farle, "Ferromagnetic resonance of ultrathin metallic layers," *Rep. Prog. Phys.* **61**, pp. 755–826 (1998); doi: 10.1088/0034-4885/61/7/001.
68. S. E. Russek, R. D. McMichael, M. J. Donahue, and S. Kaka, "High speed switching and rotational dynamics in small magnetic thin film devices," in *Spin Dynamics in Confined Magnetic Structures II*, Topics in Applied Physics, eds. B. Hillebrands and K. Ounadjela, vol. 87, Springer, Berlin, 2003, pp. 93- 154.
69. D. Ralph and M. Stiles, "Spin transfer torques," *J. Magn. Magn. Mater.* **320**, pp. 1190–1216 (2008); doi: 10.1016/j.jmmm.2007.12.019.
70. G. Bertotti, I. D. Mayergoyz, and C. Serpico, *Nonlinear Magnetization Dynamics in Nanosystems*, Elsevier Science, Amsterdam, 2008.